Atmos. Meas. Tech. Discuss., doi:10.5194/amt-2017-83, 2017
Manuscript under review for journal Atmos. Meas. Tech.
Discussion started: 30 March 2017

Atmospheric Measurement Techniques Discussions

An electrospray chemical ionization source for real-time measurement of atmospheric organic and inorganic vapors

Yue Zhao,[1] Jeremy Chan,[1,2] Felipe D. Lopez-Hilfiker,[1,3] Jeff Riffell,[2] and Joel A. Thornton[1]

[1]Department of Atmospheric Sciences, University of Washington, Seattle, WA 98195, USA

[2]Department of Biology, University of Washington, Seattle, WA 98195, USA

[3]Laboratory of Atmospheric Chemistry, Paul Scherrer Institute, 5232 Villigen, Switzerland

Correspondence to: Joel A. Thornton (thornton@atmos.washington.edu), Felipe D. Lopez-Hilfiker (felipe.lopez@psi.ch)

Atmos. Meas. Tech. Discuss., doi:10.5194/amt-2017-83, 2017
Manuscript under review for journal Atmos. Meas. Tech.
Discussion started: 30 March 2017

Atmospheric Measurement Techniques Discussions

Abstract

We present an electrospray ion source coupled to an orthogonal continuous-flow atmospheric pressure chemical ionization region. The source can generate intense and stable currents of several specific reagent ions using a range of salt solutions prepared in methanol, thereby providing both an alternative to more common radioactive ion sources and allowing for the generation of reagent ions that are not available in current chemical ionization mass spectrometry (CIMS) techniques, such as alkali metal cations. We couple the orthogonal electrospray chemical ionization (ESCI) source to a high resolution time-of-flight mass spectrometer (HRToF-MS), and assess instrument performance through calibrations using nitric acid (HNO_3), formic acid (HCOOH), and isoprene epoxydiol (*trans*-β-IEPOX) gas standards, and through measurements of oxidized organic compounds formed from ozonolysis of α-pinene in a continuous-flow reaction chamber. When using iodide as the reagent ion, the HRToF-ESCIMS prototype has a sensitivity of 11, 2.4, and 10 cps $pptv^{-1}$ per million cps of reagent ions and a detection limit (3σ, 5s averaging) of 4.9, 12.5, and 1.4 pptv to HNO_3, HCOOH, and IEPOX, respectively. These values are comparable to those obtained using an Iodide-adduct HRToF-CIMS with a radioactive ion source and low pressure ion-molecule reaction region. Applications to the α-pinene ozonolysis system demonstrates that HRToF-ESCIMS can generate multiple reagent ions (e.g, I^-, NO_3^-, acetate, Li^+, Na^+, K^+, and NH_4^+) having different selectivity to provide a comprehensive molecular description of a complex organic system.

Atmos. Meas. Tech. Discuss., doi:10.5194/amt-2017-83, 2017
Manuscript under review for journal Atmos. Meas. Tech.
Discussion started: 30 March 2017

Atmospheric Measurement Techniques Discussions

1. Introduction

The Earth's atmosphere contains thousands of inorganic and organic species that, through complex free radical and multiphase chemistry, play a vital role in air quality and climate change (Finlayson-Pitts and Pitts, 2000; Seinfeld and Pandis, 2006; Goldstein and Galbally, 2007). Characterizing the identity and abundance of many of these species in the atmosphere is essential for understanding their atmospheric processes and subsequent environmental and climate impacts. As a result, there is a critical interest in the development and application of the state-of-art analytical instruments for the analysis of atmospheric composition (Noziere et al., 2015).

As a sensitive, selective, and soft-ionization measurement technique, chemical ionization mass spectrometry (CIMS) has received significant use in the real-time *in situ* measurement of atmospheric trace species (Huey et al., 1995; Fortner et al., 2004; Hearn and Smith, 2004; Smith et al., 2004; Crounse et al., 2006; Huey, 2007; Veres et al., 2008; Kercher et al., 2009; Zhao et al., 2010). The recent coupling of chemical ionization to high resolution time-of-flight mass spectrometers (HRToF-MS) enables the simultaneous determination of the abundance and molecular composition of a wide array of atmospheric inorganic and organic compounds with fast time response and high sensitivity (Junninen et al., 2010; Bertram et al., 2011; Yatavelli et al., 2012; Aljawhary et al., 2013; Lee et al., 2014; Lopez-Hilfiker et al., 2014; Brophy and Farmer, 2015, 2016; Lopez-Hilfiker et al., 2016a; Yuan et al., 2016). The use of HRToF-CIMS has allowed groundbreaking progress in atmospheric organic chemistry, such as the observation of highly oxygenated molecules (HOMs) formed by monoterpene oxidation (Ehn et al., 2014; Jokinen et al., 2015; Berndt et al., 2016; Lee et al., 2016).

In CIMS, the analyte molecule reacts with a specific reagent ion via one or more mechanisms, including ligand switching reaction forming an ion-molecule adduct (Huey et al., 1995; Kercher et al., 2009; Aljawhary et al., 2013; Lee et al., 2014; Brophy and Farmer, 2015, 2016), proton addition (abstraction) forming a protonated (deprotonated) ion (Veres et al., 2008; Yatavelli et al., 2012; Aljawhary et al., 2013; Brophy and Farmer, 2015, 2016; Yuan et al., 2016), or by direct charge transfer forming a molecular ion (Huey et al., 1995; Kim et al., 2016). The reagent ions used mainly include I^-, NO_3^-, acetate, CF_3O^-, and SF_6^- for negative ion CIMS, and H_3O^+, NO^+, and benzene cation for positive ion CIMS. Choosing an appropriate reagent ion is essential for a comprehensive characterization of a specific class of molecules while having selectivity to avoid unnecessary congestion of the mass spectrum with unwanted components. For example, previous studies using NO_3^- CIMS have reported a very low yield of HOMs from OH oxidation of monoterpene (Jokinen et al., 2015). However, a recent study using acetate CIMS found a significantly higher HOMs yields from the same system (Berndt et al., 2016). The reason for this difference is presumably a lower sensitivity of NO_3^- to HOMs formed in OH oxidation of monoterpene than that of acetate (Berndt et al., 2016). On the other hand, many atmospheric organic systems consist of a wide range of organic compounds with different functionality and polarity. Therefore, multiple complementary ionization schemes are needed to obtain a broad view of these systems (Aljawhary et al., 2013; Praplan et al., 2015).

Atmos. Meas. Tech. Discuss., doi:10.5194/amt-2017-83, 2017
Manuscript under review for journal Atmos. Meas. Tech.
Discussion started: 30 March 2017

Atmospheric Measurement Techniques Discussions

Some advantages of CIMS are that it is direct, online, reproducible and inherently quantitative in that the kinetic theory of gases allows a robust upper limit ionization efficiency, and thus instrument response, to be calculated knowing only the pressure and interaction time of reagent ions and analyte molecules.. However, the need for gas-phase reagent ions limits the suite of usable reagent ions to those for which a safe and stable gas-phase precursor exists and which produce the desired reagent ion cleanly at a high yield when ionized. As such, certain reagent ions such as metal cations (e.g., Na^+, K^+, and NH_4^+), which are commonly used for detection of atmospheric organic compounds in off-line techniques like electrospray ionization (ESI)-MS (Nizkorodov et al., 2011; Laskin et al., 2012; Witkowski and Gierczak, 2013), have remained largely unavailable for CIMS (Fujii et al., 2001). Compared to I^-, NO_3^-, and acetate, these metal cations are expected to be less selective toward oxidized organic compounds and can be used to sensitively detect both less oxidized (e.g, compounds containing only carbonyl groups) and highly polar multi-functional organic species (Gao et al., 2010; Nguyen et al., 2010; Nizkorodov et al., 2011; Laskin et al., 2012; Witkowski and Gierczak, 2013; Zhao et al., 2015; Tu et al., 2016; Zhao et al., 2016). In addition, at present most CIMS techniques use a radioactive ion source such as Po-210 to produce the reagent ions, although more recently some utilize X-ray radiation, electrical discharge (Hirokawa et al., 2009; Yuan et al., 2016), or electron impact (Inomata and Hirokawa, 2017). Safety regulations for the transport and use of radioactive materials may limit the deployment of the instrument with a radioactive ion source in the field, while other methods may be less intense or lead to higher backgrounds.

We have developed a non-radioactive reagent ion source that deploys a custom-built electrospray setup within an atmospheric pressure orthogonal ion-molecule reaction (IMR) chamber. The design of the IMR region is similar to that of the Cluster-CIMS developed by Eisele and coworkers (Zhao et al., 2010). The electrospray chemical ionization (ESCI) source is coupled to a HRToF-MS for characterization. We present the design and discuss the parameters most important for optimal performance of the ESCI source. Then, we assess its performance using the measurement of formic acid, IEPOX, nitric acid, and organic mixtures formed by ozonolysis of α-pinene in a continuous-flow reaction chamber. Our results demonstrate that the ESCI source provides a potential alternative to radioactive and X-ray ion source and opens a new avenue for the generation of reagent ions such as Li^+, Na^+, K^+, and so on, that were previously unavailable for CIMS.

2. Experimental

2.1 Instrument description

A schematic of the ESCI module is shown in Figure 1. The electrospray setup contains a 15 μm inner diameter (ID) fused silica spray needle mounted within a cylindrical evaporation chamber through which a flow of ultra-high purity (UHP) N_2 (referred to as the ion source flow) is passed to aid in the evaporation of the spray droplets and to transport ions into the IMR. Several spray needle diameters were tried (from 8 to 30 μm), with the 15 μm giving the best combination of

longevity and ion intensity. The emitting end of the spray needle is located 4 mm from the distal wall of the evaporation chamber, which consists of a 13 mm ID stainless steel (SS) tube welded to the center of a circular SS aperture having a 4 mm diameter. The aperture forms the entrance into the IMR which is a portion of a 22 mm ID SS tube embedded in a Teflon block. The ion source flow enters the IMR through the aperture perpendicularly to the direction of a much larger sample flow, typically 10 to 20 standard liters per minute (slpm) drawn through the IMR by a pump. Preliminary fluid dynamic simulations suggest that the mixed sample and ion source flow in the IMR remains laminar when the ratio of the ion source flow to sample flow is ≤ 0.2 and the overall Reynolds number for the sample flow is low (sample flow < 20 slpm).

Ions are driven across the perpendicular sample flow to a SS capillary tube located on the opposite wall of the IMR by means of a 2 to 4 kV potential between the evaporation region lens and the capillary tube. The SS capillary projects 3.5 mm into the IMR and acts as the atmospheric pressure interface between the IMR and the vacuum chamber of a commercial HRToF-MS (Tofwerk AG, Thun, Switzerland). The HRToF-MS and its data acquisition procedures have been described in detail previously (Junninen et al., 2010; Bertram et al., 2011; Lee et al., 2014). The evaporation tube, lens and IMR tube are electrically connected, while the mass spectrometer entrance capillary is electrically isolated from the IMR by a ~1 mm thick jacket of Teflon.

During operation, a dilute salt solution (~0.05 wt%) in HPLC-grade methanol (MEOH) is biased at the reservoir to ~ 3 to 5 kV. The reservoir is maintained at approximately 50 mbar above atmosphere using a commercial pressure controller (FLUIGENT, model MFCS-EZ) with 0.05 mbar precision. Under laminar flow conditions, the reaction time between reagent ions and sampled trace gases in the IMR is mainly determined by the electric field-induced drift velocity of the reagent ions. For instance, for two reagent ions used in this study, NO_3^- and Na+, the ion-molecule reaction time (i.e., ion drift time) in the IMR is estimated to be 0.5-1 ms and 0.4-0.7 ms, respectively, with an ion mobility of 2.37 $cm^2\ s^{-1}\ V^{-1}$ for NO_3^- (Ellis et al., 1978) and 3.4 $cm^2\ s^{-1}\ V^{-1}$ for Na^+ (Bohringer et al., 1987) under typical operation conditions (2-4 kV across the IMR).

The ion source and sample flow rates can significantly affect the performance of the ion source. The ion source flow can aid in the generation and transport of the reagent ions into the IMR, but it may disrupt the initially laminar sample flow, especially when the sample flow is small. However, at large sample flows, the time for the ions to exit the IMR via the sample flow may be comparable to the ion drift time across the IMR at a constant potential. As a result, the sample flow may carry away the reagent ions as well as ion-molecule clusters, lowering the apparent ionization efficiency. Therefore, the ion source flow and sample flow need to be carefully optimized.

For comparison purposes, our prototype source was designed such that it could incorporate a commercial 10 mCi Po-210 inline ion source (NRD LLC) as in more typical low-pressure CIMS instruments used for atmospheric composition studies (see introduction). With CH_3I in UHP N_2

Atmos. Meas. Tech. Discuss., doi:10.5194/amt-2017-83, 2017
Manuscript under review for journal Atmos. Meas. Tech.
Discussion started: 30 March 2017

Atmospheric Measurement Techniques Discussions

as a reagent ion source, this set up was able to produce 0.6-1.8 × 10^6 cps of reagent ions at atmospheric pressure using an ion source flow rate of 1-2 slpm and a sample flow rate of 10 slpm, with >2 kV potential across the IMR. Although the commercial Po-210 sources are not optimized for ion transmission at low flow rates and high pressures, this intensity is certainly suitable for use in field or laboratory studies.

2.2 Laboratory characterization

2.2.1 Generation of reagent ions and calibration gas standards

In this study, three negative (i.e., I^-, NO_3^-, and acetate) and four positive reagent ions (i.e., Li^+, Na^+, K^+, and NH_4^+) were generated by electrospraying their precursor salt solutions prepared in HPLC grade MEOH (Fisher Scientific). Sodium iodide (≥ 99.5%, EMD), sodium nitrate (≥ 99%, Mallinckrodt), potassium acetate (AR(ACS), Macron), ammonium acetate (99.2%, Fisher chemical), and lithium chloride (≥ 99%, Mallinckrodt) were used to produce I^- and Na^+, NO_3^-, K^+ and acetate, $NH4^+$, and Li^+ respectively. All the salts were used as received.

Three calibration gases, i.e., nitric acid (HNO_3), isotope-labeled formic acid ($H^{13}COOH$), and isoprene epoxydiols (*trans*-β-IEPOX) were used to calibrate the instrument. Gases of nitric acid and formic acid were generated using a custom-built PTFE permeation tube containing respective acid liquids, kept constantly at 40 ^oC. The permeation rate was determined gravimetrically. IEPOX vapor was generated by passing a flow of UHP N_2 over ~200 µl IEPOX solution in ethyl acetate kept in a glass bulb at room temperature. The concentration of IEPOX in the flow exiting the bulb was determined by an Iodide-adduct HRToF-CIMS employing a radioactive ion source, for which the sensitivity to IEPOX was calibrated using the method as described previously (Lee et al., 2014). These three gases are common in the atmosphere and span a range in their properties important for CIMS such as acidity, polarity, and size.

2.2.2 Optimization of operation conditions, calibration, and background determination

The influence of sample flow and ion source flow on the ion signals was systematically evaluated using I^- as the reagent ion. The room air was directly sampled into the IMR at a flow rate ranging from 2-20 standard liters per minute (slpm). At each sample flow rate, the ratio of ion source flow/sample flow is varied from 0.02-0.2. The HNO_3 and $H^{13}COOH$ gases were added to the sample flow during the optimization.

Calibrations with HNO_3, $H^{13}COOH$, and IEPOX were performed using I^- reagent ions under optimized sample flow and ion source flow conditions. Atmospherically relevant concentrations of the calibration gases were obtained by varying the dilution of the source gas in UHP N_2 prior to delivery in the sample flow. The observed ion signals as a function of gas concentration allow the determination of the instrument sensitivity. In addition, the sample flow was humidified to a wide range of relative humidity (0-80% RH, corresponding to water vapor pressure, P_{H2O}, of 0-25 mbar) to explore the influence of water vapor on the instrument sensitivity. The determined

Atmos. Meas. Tech. Discuss., doi:10.5194/amt-2017-83, 2017
Manuscript under review for journal Atmos. Meas. Tech.
Discussion started: 30 March 2017

Atmospheric Measurement Techniques Discussions

sensitivities as well as the dependence on P_{H2O} were compared to the measurements by a radioactive Iodide-adduct HRToF-CIMS. The background signals of the instrument were determined routinely by directly sampling dry UHP N_2.

2.2.4 Chamber experiments of α-pinene ozonolysis

The capability of the instrument for characterizing atmospherically relevant complex organic systems was evaluated by measuring the oxidation products from α-pinene ozonolysis using seven different reagent ions described above. Experiments of α-pinene ozonolysis were carried out in a 0.75 m^3 PTFE chamber operated in a continuous-flow mode at the University of Washington. The chamber was first flushed by 12 slpm of zero air generated by a Teledyne zero air generator (Model 701) for >72 h. Ozone, generated by flowing ultra-zero air (Praxair) at 5 sccm (standard cubic centimeter per minute) past a mercury lamp, was delivered to the chamber during the zero air flushing. α-Pinene was then added by flowing 100 sccm of UHP N_2 through a glass diffusion tube containing pure α-pinene and kept in a methanol cold trap at -70 ^oC. The initial concentrations of O_3 and α-pinene added in the chamber were approximately 75 and 110 ppbv, respectively. The oxidation products formed in the chamber were sampled at 10 slpm by the HRToF-ESCIMS after 48 h of chamber equilibration.

3. Results and Discussion

3.1 Ion source and sample flow optimization

Figure 2a shows an example using iodide reagent ions of ion signal dependence on the ion source flow rate during sampling of humid air (P_{H2O} = 15 mbar) at 10 slpm containing an added $H^{13}COOH$ standard. As expected, the reagent ion (I^- and $I(H_2O)^-$) signals increase with increasing ion source flow. The increase of the signal for $I(H^{13}COOH)^-$ is well correlated with that of the reagent ions. The positive effect of the ion source flow is likely due to more efficient evaporation and transport of reagent ions from the spray evaporation region into the IMR region.

Figure 2b shows the ion signals for I^-, $I(H_2O)^-$, $I(H^{13}COOH)^-$, and $I(HNO_3)^-$ observed during sampling of humid air (P_{H2O} = 15 mbar) containing $H^{13}COOH$ and HNO_3 standards at a sample flow rate ranging from 2-20 slpm. The corresponding ion source flow was controlled to always be 1/10 of the sample flow. All ion signals increase initially with the increase of the sample flow, reach maximum values at 12 slpm, and then decrease slightly with further increase of the sample flow. At small sample flows, the time for the sample flow to pass through the IMR is long compared to electric field-induced ion drift time across the IMR region, and so the influence of the sample flow upon ion transit across IMR should be small. However, the corresponding increase of the ion source flow with the sample flow can promote the generation and transmission of reagent ions into the IMR, thus leading to the increase of ion signals. At large sample flows, the influence of the sample flow on the ion transit across IMR becomes significant and is no longer compensated by the enhancement in ion signals due to the increased ion source flow, hence resulting in a decrease in ion signals.

Atmos. Meas. Tech. Discuss., doi:10.5194/amt-2017-83, 2017
Manuscript under review for journal Atmos. Meas. Tech.
Discussion started: 30 March 2017

Atmospheric Measurement Techniques Discussions

For the characterizations and applications discussed below, the sample flow and ion source flow are kept at 10 slpm and 1 slpm, respectively as these are reasonable conditions for use on environmental simulation chambers and in field measurements. We note that the sample flow can be extended to up to 20 slpm without significant loss of ion signal, and the optimal ion source flow of 2 slpm is essentially the same UHP N_2 flow requirement for current Po-210 based ion sources (Lee et al., 2014). Further improvements in the spray environment and associated transfer optics will likely further minimize the ion source flow.

3.2 Sensitivity to selected trace gases

To assess the performance of the HRToF-ESCIMS, we measured the sensitivity to HNO_3, $H^{13}COOH$, and IEPOX using I^- as the reagent ion. The iodide-based CIMS has been widely used to detect atmospheric inorganic and organic compounds in previous studies (Huey et al., 1995; Kercher et al., 2009; Lee et al., 2014; Brophy and Farmer, 2015; Lee et al., 2016; Lopez-Hilfiker et al., 2016b), though almost exclusively at low pressure (20 – 80 mbar) as opposed to the atmospheric pressure (1013 mbar) implementation used here. The sensitivity of iodide-based CIMS to a given compound mainly depends on the polarity and hydrogen binding energy of a compound to the I^- ion (Lee et al., 2014; Iyer et al., 2016). In the atmospheric pressure ESCIMS, the ion molecule reaction time is set by the electric field, and is up to a factor of 30 or more shorter than those in low-pressure CIMS instruments. The shorter reaction time should linearly lower sensitivities. However, the ion-molecule collision frequency is more than a factor of 10 higher in the atmospheric pressure ESCIMS for the same ambient concentrations of analytes. Thus, we would expect the ESCIMS sensitivities to be only slightly lower than those found in the low-pressure CIMS. It is possible that adduct formation is further stabilized by third-body effects and that the ESCIMS could in fact have higher sensitivities for some compounds forming weaker clusters.

Figure 3 shows the signals of $I(HNO_3)^-$, $I(H^{13}COOH)^-$, and $I(IEPOX)^-$ per million reagent ion count rate at different atmospherically relevant concentrations of the standards under dry and humid conditions. The signal response is linear within the investigated concentration range for all three trace gases, with the slope of the linear fit to the ion signals corresponding to the sensitivity per million reagent ion count rate. The HRToF-ESCIMS exhibits a sensitivity of 11, 2.4, and 10 cps $pptv^{-1}$ to HNO_3, HCOOH, and IEPOX, respectively, under dry conditions and 9.1, 0.5, and 1.7 cps $pptv^{-1}$, respectively, under humid conditions (P_{H2O} = 14 or 15 mbar). These sensitivities, and those that follow are given per million cps of reagent ion. Lee et al. (2014) explored the sensitivity of a low-pressure Iodide-adduct HRToF-CIMS equipped with a radioactive ion source to a number of atmospheric inorganic and organic compounds. They reported sensitivities to HNO_3, HCOOH, and IEPOX of 4.0, 2.9, and 0.39 cps $pptv^{-1}$, respectively, at 0.2 mbar water vapor pressure in IMR. Using the same instrument as used by Lee et al. (2014), we have more recently obtained higher values of sensitivities to HCOOH (7 cps $pptv^{-1}$) and IEPOX (10 cps $pptv^{-1}$) in the laboratory. Thus, the atmospheric-pressure ESCIMS and low-pressure CIMS approaches are fairly similar in response to the same compounds. The

Atmos. Meas. Tech. Discuss., doi:10.5194/amt-2017-83, 2017
Manuscript under review for journal Atmos. Meas. Tech.
Discussion started: 30 March 2017

Atmospheric Measurement Techniques Discussions

sensitivity difference in these calibrations is likely attributed to the differences in instrument parameters, including the configurations and pressures of the ion source and IMR, and the ion optic settings within the vacuum chamber that strongly affect ion transmission to the mass spectrometer.

The presence of water vapor can affect sensitivities, either by competing for I^- ions, thus lowering the sensitivity, or by accommodating excess energy from the collision to stabilize the Iodide-molecule clusters, thereby increasing the sensitivity (Lee et al., 2014; Iyer et al., 2016). Moreover, water vapor can affect the transmission of soluble gases through sample tubing. In the current configuration of the ESCIMS, it is difficult to separate these two effects experimentally as done previously in low-pressure IMR regions by using separate delivery lines for calibrants and water vapor. Thus, our results shown here reflect both ionization efficiency and sample transfer aspects because the sample flow delivering the calibrants had to be humidified.

Figure 4 shows the dependence of the instrument sensitivities to HNO_3, $H^{13}COOH$, and IEPOX on the P_{H2O} of the sample flow. The sensitivities to HNO_3, $H^{13}COOH$, and IEPOX increase initially with the addition of water vapor at lower P_{H2O}, reach the maximum values at 4.1, 2.2, and 2.2 mbar, respectively, and then decrease with the further increase of P_{H2O}. Compared to HNO_3 and $H^{13}COOH$, the positive water vapor effect on the sensitivity at low P_{H2O} for IEPOX is significantly smaller. Lee et al. (2014) investigated the effects of water vapor on the sensitivity of a low-pressure Iodide-adduct HRTOF-CIMS in the P_{H2O} (water vapor pressure in IMR) range of 0-0.8 mbar, and found a positive water vapor dependence for the sensitivity to HNO_3 and an approximately inverse U-shaped dependence for the sensitivity to HCOOH. In general, the trends for the sensitivities to HNO_3 and HCOOH versus P_{H2O} observed by Lee et al. are consistent with those at $P_{H2O} \leq 4.1$ mbar observed in the present study. In addition, recent measurements using the same low-pressure Iodide-adduct HRTOF-CIMS in our lab show that the addition of water vapor with P_{H2O} of 0.26 Torr has no significant impacts on the sensitivity to IEPOX, consistent with the relatively weak humidity dependence of the sensitivity to IEPOX at low P_{H2O} observed in the present study. The sharp decrease in the sensitivities at higher P_{H2O} as seen in Figure 4 is therefore likely a result of the competitive consumption of I^- ions by water vapor, which dominates over the kinetic stabilization effect of water for the ion-molecule clusters, as well as a larger wall partitioning in the ~50 cm sampling tube under these conditions.

3.3 Instrument backgrounds and detection limits

The background signals for the instrument arise mainly from the impurities in the electrospray solvent and the salts used for the generation of reagent ions, as well as the desorption of gas species adsorbed onto the wall of the sampling tube and IMR. The instrument backgrounds were routinely measured by sampling UHP N_2. Figure 5 shows a typical high-resolution mass spectrum in the I^- mode recorded when sampling UHP N_2. The spectrum recorded during the addition of HNO_3, $H^{13}COOH$, and IEPOX to the UHP N_2 flow is also displayed for comparison. The typical backgrounds for HNO_3, $H^{13}COOH$, and IEPOX were measured to be 800, 240, and

Atmos. Meas. Tech. Discuss., doi:10.5194/amt-2017-83, 2017
Manuscript under review for journal Atmos. Meas. Tech.
Discussion started: 30 March 2017

Atmospheric Measurement Techniques Discussions

50 cps, respectively. It is noted that the instrument backgrounds can be reduced by using higher purity electrospray solvents and reagent ion precursor salts, or by using a larger sample flow that can dilute the background concentration of the species desorbed from the wall. Moreover, many experiments adding large concentrations of these standards to the sampling tube had been performed over months, and thus it is likely that these backgrounds are anomalously high.

Assuming the uncertainty in the signal and background follows Poisson counting statistics, the signal to noise (*S/N*) ratio can be determined from eq. (1) (Bertram et al., 2011):

$$\frac{S}{N} = \frac{C_f[X]t}{\sqrt{C_f[X]t + 2Bt}} \quad (1)$$

Where C_f is the instrument sensitivity; *[X]* is the concentration for a trace gas; *B* is the background count rate; *t* is the integration time. We define the detection limit of the HRToF-ESCIMS for a trace gas as the concentration that gives rise to an *S/N* ratio of 3. Using the measured instrument sensitivities and backgrounds, we calculate a detection limit of 4.9, 12.5, and 1.4 pptv for HNO_3, $H^{13}COOH$, and IEPOX, respectively, for 5s averaging, in the I^- mode. These limits of detection are comparable to those for a low-pressure Iodide-adduct HRTOF-CIMS in our lab (Lee et al., 2014).

3.4 Application to chamber studies of α-pinene ozonolysis

3.4.1 Raw mass spectra

Gas mixtures formed by ozonolysis of α-pinene in a steady-state chamber were used to assess the capabilities of this technique for characterizing complex organic systems of atmospheric relevance. Three negative ions (i.e., I^-, NO_3^-, acetate) and four positive ions (i.e., Li^+, Na^+, K^+, NH_4^+) were used as regent ions for measurements. High resolution peak fitting was performed and reasonable molecular formulae were assigned for detected ions that have intensity higher than 5 cps in all seven ion modes. Many ions are present at < 5 cps, which might be of importance to various mechanisms of particle growth or organic radical chemistry, but the compositions of these ions is beyond the scope of this paper. Overall, the results show that the ions observed in NO_3^- and four positive ion modes are in the form of ion-molecule clusters, whereas those observed in I^- and acetate modes are either ion-molecule clusters or molecular ions. The iodide clusters can be easily distinguished from iodide-free molecular ions due to the large negative mass defects of iodide (Lee et al., 2014), whereas broadly distinguishing between acetate clusters and deprotonated molecule ions remains a challenge when not using isotopically labeled acetate as the reagent ion. Therefore, while chemical formulae for the ions can be obtained, their attribution to a product of α-pinene ozonolysis cannot be made with high confidence (Lopez-Hilfiker et al., 2015; Brophy and Farmer, 2016).

Examples of high-resolution mass spectra of α-pinene ozonolysis products derived in I^- and NO_3^- modes are given in Figure 6 and the spectra obtained in four positive ion modes are given in

Atmos. Meas. Tech. Discuss., doi:10.5194/amt-2017-83, 2017
Manuscript under review for journal Atmos. Meas. Tech.
Discussion started: 30 March 2017

Atmospheric Measurement Techniques Discussions

Figure 7. The iodide-mode mass spectrum of the ozonolysis products obtained here is similar to that obtained using the low-pressure Iodide-adduct HRToF-CIMS as discussed previously (Lopez-Hilfiker et al., 2015). It can be seen that peaks assigned to monomeric products ($\leq C_{10}$) are apparent in all ion modes, while peaks associated with dimeric species are evident only in the positive ion mode (discussed further below). Peak distributions in both monomer and dimer regions is very similar for Li^+, Na^+, K^+, and NH_4^+, suggesting these positive ions likely have a similar selectivity to α-pinene ozonolysis products. It is interesting to note that in negative ion modes, ion clusters of precursor salt molecules (e.g., $I(NaI)^-$ and $NO_3(NaNO_3)_n^-$) were observed with high intensities. These ions can be used as excellent mass calibration species.

3.4.2 Mass defect plots

To better compare the sensitivity and selectivity between this subset of negative and positive reagent ions, the mass defects of identified products are plotted against their exact mass for I^-, NO_3^-, and Na^+ modes. Figure 8 shows the comparisons of mass defect plots between I^- (or NO_3^-) mode and Na^+ mode. In the mass defect plots, the green, yellow, and purple open circles represent the products observed only in one ion mode and their size is proportional to the signal intensity of observed clusters. The blue open markers in the plots represent the products identified in both ion modes of comparison and their size is proportional to the square root of the pinic acid-normalized signal intensity ratio (R) between the two ion modes:

$$R = \frac{S_{A^-,i}/S_{A^-,PA}}{S_{Na^+,i}/S_{Na^+,PA}} \quad (2)$$

Where, $S_{A^-,i}$ and $S_{A^-,PA}$ are the signal intensity of clusters for product i and pinic acid in I^- (or NO_3^-) mode, respectively; $S_{Na^+,i}$ and $S_{Na^+,PA}$ are the signal intensity of product i and pinic acid in Na^+ mode, respectively. As pinic acid ($C_9H_{14}O_4$) is among the most abundant products observed in I^-, NO_3^-, and Na^+ modes (see Figures 6 and 7), the value of R (i.e., the size of the markers relative to that for pinic acid (red solid circles)) can be an indicator of the relative sensitivity of I^- (or NO_3^-) and Na^+ to the oxidation products.

In the monomer region of the mass defect plots, the less oxidized products observed in both modes of comparison generally have a value of $R \leq 1$ (the blue markers have sizes smaller than or close to that of pinic acid). Thus, Na^+ is generally more sensitive to less oxidized species than I^- and NO_3^-, and most of products observed only in the Na^+ mode show very low oxygen contents ($n_O \leq 3$). As many of these species have signal intensities larger than 1000 cps, their absence in I^- and NO_3^- modes suggests that I^- and NO_3^- are extremely insensitive to these least oxidized species, in agreement with the observations in previous studies (Lee et al., 2014; Hyttinen et al., 2015; Iyer et al., 2016). In contrast, the more oxidized products observed in both modes of comparison show a wide range of R values (e.g, $R \leq 1$ or $R \geq 1$, corresponding to the blue markers having sizes smaller or larger than that of pinic acid). This indicates that I^-, NO_3^-, and Na^+ are all sensitive to more oxidized species but have different sensitivities to a specific species.

Atmos. Meas. Tech. Discuss., doi:10.5194/amt-2017-83, 2017
Manuscript under review for journal Atmos. Meas. Tech.
Discussion started: 30 March 2017

Atmospheric Measurement Techniques Discussions

In fact, some highly oxidized products having high oxygen contents ($n_O \geq 5$) are observed only in one of these three ion modes. Note that most of these products have signal intensities lower than 50 cps, suggesting that they likely have very low concentrations, which are below the detection limit in the other two modes.

The selectivity of I^- and NO_3^- toward more oxidized species as suggested here is consistent with the observations in previous studies (Lee et al., 2014; Berndt et al., 2016), which showed that these two reagent ions can have distinct sensitivities to the oxidized species having similar oxygen contents, depending on the identities and locations of the functional groups. It is clear in Figure 8 that some very small species (e.g., CH_2O_2, CH_2O_3, $C_2H_2O_3$, and $C_2H_4O_3$) have a value of R significantly larger than 1, indicating that I^- and NO_3^- are markedly more sensitive to these small species than is Na^+.

Comparisons of the mass defect plots in the dimers region show a large difference in the detection of the gas-phase dimers between I^- (or NO_3^-) and Na^+ modes. These dimers have compositions ranging, for example, from $C_{15}H_{26}O_3$ to $C_{20}H_{32}O_7$. We note that many of these dimers have been recently detected in the gas-phase using a low-pressure Iodide-adduct HRToF-CIMS in a boreal forest environment (Mohr et al., 2017). Thus, while the lower detection efficiency of dimers in this work using I^- or NO_3^- may be from differences in reagent ion sensitivities, we suspect that differences in ion optic settings between negative and positive ion modes that affect ion transmission efficiencies at large mass-to-charge ratios is a more likely explanation. These settings were not optimized in this work, and improvements to high mass transmission in negative ion mode are ongoing. Therefore, we refrain from concluding about the relative detection efficiency of dimers in negative ion mode using the atmospheric pressure ESCI.

In summary, these comparisons suggest that there is not a reagent ion that captures all components of α-pinene ozonolysis with equally high sensitivity. Therefore, to gain a comprehensive view on a complex organic system, a combination of reagent ions with different selectivity is needed.

3.4.3 Declustering scans

Ion-molecule clusters, depending on their binding energies, may break apart due to collision-induced dissociation (i.e., declustering) during transmission through the ion optics within the vacuum chamber. In general, clusters with stronger binding energies can more easily survive declustering in the vacuum chamber, thus the instrument likely has higher sensitivities to the corresponding analytes, and the observed sensitivities should be closer to those calculated by ion-molecule collision rates. Declustering scanning, which is performed by systematically increasing the voltage difference (ΔV) between first and the second quadrupole sections of the MS, allows for insights into the binding energies of clusters (Lopez-Hilfiker et al., 2016a). Figure 9 shows the declustering scans of clusters containing $C_{10}H_{16}O_{2\text{-}8}$ and $C_9H_{14}O_{3\text{-}8}$ products in I^- and NO_3^- modes. It is clear that, with the increase of electrical field strength, the cluster

signals for products having higher oxygen contents generally decay more slowly than those having lower oxygen contents. This is consistent with the fact that I^- and NO_3^- ions generally bind more strongly to compounds containing more hydroxy or hydroperoxy moieties (Lee et al., 2014; Hyttinen et al., 2015; Iyer et al., 2016). We note that the trends of decay for $C_{10}H_{16}O_{2\text{-}8}$ iodide clusters are in excellent agreement with previous measurements using a low-pressure iodide-adduct HRToF-CIMS (Lopez-Hilfiker et al., 2016a).

Declustering scans in Li^+, Na^+, K^+, and NH_4^+ modes show that the cluster signals for the most abundant monomeric products such as $C_{10}H_{16}O_{2\text{-}5}$ and $C_9H_{14}O_{2\text{-}5}$ increase initially with increasing ΔV and then decrease with further increase of ΔV. The initial increase in cluster signals may be associated with ion transmission efficiency of the instrument. As the small positive regent ions have very low transmission efficiencies through the ion optics, the concentration of the reagent ions in the vacuum chamber may be low. As a result, the declustering of reagent ion-water and -precursor salt molecule clusters may greatly increase the concentration of reagent ions in the vacuum chamber. These reagent ions may quickly bind to the neutral oxidation products that are present in larger abundance, leading to the increase of their cluster signals. Here, we use the declustering scans of dimers instead of C_9 and C_{10} monomers to compare the binding energies of four positive reagent ions.

As can be seen in Figure 10, the decay rate of the cluster signals in four positive ion modes follows the order: $NH_4^+ > K^+ > Na^+ > Li^+$. This indicates an order of $Li^+ > Na^+ > K^+ > NH_4^+$ for the binding energies of the clusters, consistent with expectations from charge density considerations. In each ion mode, the cluster signals for smaller dimers generally decay more slowly than those for larger dimers, suggesting these positive ions can more strongly bind to the smaller dimers, likely due to the higher polarity or the smaller steric effect for smaller dimers. It is worth noting that none of the clusters signals drop with the increase of ΔV up to 10 and 6 V in Li^+ and Na^+ modes, respectively. This behavior implies these dimers are most likely covalently-bound species formed during α-pinene ozonolysis, rather than noncovalently-bound species formed due to ion-induced clustering in the instrument, which are not expected to survive at strong declustering strengths. To our knowledge, this result is the first direct confirmation that these dimeric products are strongly bound, providing important support for the interpretation that the detected ions represent real gas-phase products of α-pinene oxidation (Ehn et al., 2012; Zhao et al., 2013; Ehn et al., 2014; Kristensen et al., 2016; Trostl et al., 2016; Mohr et al., 2017)

4. Conclusion

We report an electrospray chemical ionization (ESCI) source coupled to a HRToF-MS for the real-time online measurement of atmospheric organic and inorganic species in the gas-phase. The ESCI source is unique in that it does not rely on radioactive materials or X-ray radiation that are subject to safety regulations, and allows the production of reagent ions (e.g., alkaline cations) that are not available in current CIMS techniques. Calibration experiments using nitric acid, formic acid, and IEPOX gas standards show that the HRToF-ESCIMS using iodide reagent ions

has sensitivities and limits of detection comparable to those obtained for a low-pressure Iodide-adduct HRToF-CIMS using a radioactive ion source. The detection of oxidized organic compounds formed from α-pinene ozonolysis in a chamber using seven different reagent ions (e.g., I^-, NO_3^-, acetate, Li^+, Na^+, K^+, and NH_4^+) shows different selectivities for these reagent ions and expected ion-adduct binding energy trends. The data demonstrate the capability of this technique for comprehensively characterizing complex organic systems using a combination of reagent ions.

The ESCI source presented here is in its early stages of development. Continued characterization of the sensitivity and selectivity of different reagent ions, especially their dependence on humidity are needed. Further optimizations of the ion source are also required to improve its performance especially the long-time stability, which is particularly important for field applications. Versions of our prototype source allowed 10 to 24 hours of continuous operation before ion signal degraded, which is certainly suitable for many laboratory experiment durations. A short immersion of the spray tip into HPLC grade MEOH was enough to return to the same ion signal for another 10 to 24 hours, suggesting the reason was simply salt build-up on the spray needle tip altering the spray characteristics. Thus, it is likely that more dilute spray solutions, shorter spray needle tips, a conventional coaxial sheath gas flow around the needle tip, and off-axis spray geometry would greatly improve source stability. Moreover, shifting the spray source further upstream of the entrance capillary would increase ion-molecule reaction times and thus sensitivity, as in Zhao et al. (2013). Finally, applying a dry UHP N_2 counter flow at the mass spectrometer entrance capillary would prevent ambient particles and possible charged spray droplets that are not completely evaporated from entering and blocking the capillary tube. This counter flow could also prevent free water molecules entering the vacuum chamber and promote the dissociation of reagent ion-water clusters, which may lead to an increase of the instrument sensitivity, especially in positive ion mode.

Acknowledgement

This work was supported by the National Science Foundation (CHE-1404573). Jeremy Chan acknowledges the support of the University of Washignton Royalty Research Fund (Grant 65-7716). We are grateful to Dennis Canuelle, the instrument maker, for help in designing and building the ESCI source.

References

Aljawhary, D., Lee, A. K. Y., and Abbatt, J. P. D.: High-resolution chemical ionization mass spectrometry (ToF-CIMS): application to study SOA composition and processing, Atmos. Meas. Tech., 6, 3211-3224, doi:10.5194/amt-6-3211-2013, 2013.

Berndt, T., Richters, S., Jokinen, T., Hyttinen, N., Kurten, T., Otkjaer, R. V., Kjaergaard, H. G., Stratmann, F., Herrmann, H., Sipila, M., Kulmala, M., and Ehn, M.: Hydroxyl radical-induced formation of highly oxidized organic compounds, Nat Commun, 7, 13677, 2016.

Bertram, T. H., Kimmel, J. R., Crisp, T. A., Ryder, O. S., Yatavelli, R. L. N., Thornton, J. A., Cubison, M. J., Gonin, M., and Worsnop, D. R.: A field-deployable, chemical ionization time-of-flight mass spectrometer, Atmos. Meas. Tech., 4, 1471-1479, 2011.

Bohringer, H., Fahey, D. W., Lindinger, W., Howorka, F., Fehsenfeld, F. C., and Albritton, D. L.: Mobilities of several mass-identified positive and negative ions in air, Int. J. Mass Spectrom. Ion Processes, 81, 45-65, 1987.

Brophy, P., and Farmer, D. K.: A switchable reagent ion high resolution time-of-flight chemical ionization mass spectrometer for real-time measurement of gas phase oxidized species: characterization from the 2013 southern oxidant and aerosol study, Atmos. Meas. Tech., 8, 2945-2959, 2015.

Brophy, P., and Farmer, D. K.: Clustering, methodology, and mechanistic insights into acetate chemical ionization using high-resolution time-of-flight mass spectrometry, Atmos. Meas. Tech., 9, 3969-3986, doi:10.5194/amt-9-3969-2016, 2016.

Crounse, J. D., McKinney, K. A., Kwan, A. J., and Wennberg, P. O.: Measurement of gas-phase hydroperoxides by chemical ionization mass spectrometry, Anal. Chem., 78, 6726-6732, 2006.

Ehn, M., Kleist, E., Junninen, H., Petaja, T., Lonn, G., Schobesberger, S., Dal Maso, M., Trimborn, A., Kulmala, M., Worsnop, D. R., Wahner, A., Wildt, J., and Mentel, T. F.: Gas phase formation of extremely oxidized pinene reaction products in chamber and ambient air, Atmos. Chem. Phys., 12, 5113-5127, 2012.

Ehn, M., Thornton, J. A., Kleist, E., Sipila, M., Junninen, H., Pullinen, I., Springer, M., Rubach, F., Tillmann, R., Lee, B., Lopez-Hilfiker, F., Andres, S., Acir, I. H., Rissanen, M., Jokinen, T., Schobesberger, S., Kangasluoma, J., Kontkanen, J., Nieminen, T., Kurten, T., Nielsen, L. B., Jorgensen, S., Kjaergaard, H. G., Canagaratna, M., Dal Maso, M., Berndt, T., Petaja, T., Wahner, A., Kerminen, V. M., Kulmala, M., Worsnop, D. R., Wildt, J., and Mentel, T. F.: A large source of low-volatility secondary organic aerosol, Nature, 506, 476-479, doi:10.1038/nature13032, 2014.

Ellis, H. W., McDaniel, E. W., Albritton, D. L., Viehland, L. A., Lin, S. L., and Mason, E. A.: Transport properties of gaseous ions over a wide energy range. Part II, At. Data Nucl. Data Tables, 22, 179-217, 1978.

Finlayson-Pitts, B. J., and Pitts, J. N.: Chemistry of the upper and lower atmosphere: theory, experiments, and applications, Academic Press, San Diego, 2000.

Fortner, E. C., Zhao, J., and Zhang, R. Y.: Development of ion drift-chemical ionization mass spectrometry, Anal. Chem., 76, 5436-5440, 2004.

Fujii, T., Selvin, P. C., Sablier, M., and Iwase, K.: Lithium ion attachment mass spectrometry for on-line analysis of trace components in air: direct introduction, Int. J. Mass Spectrom., 209, 39-45, 2001.

Gao, Y. Q., Hall, W. A., and Johnston, M. V.: Molecular composition of monoterpene secondary organic aerosol at low mass loading, Environ. Sci. Technol., 44, 7897-7902, doi:10.1021/Es101861k, 2010.

Goldstein, A. H., and Galbally, I. E.: Known and unexplored organic constituents in the earth's atmosphere, Environ. Sci. Technol., 41, 1514-1521, doi:10.1021/Es072476p, 2007.

Hearn, J. D., and Smith, G. D.: A chemical ionization mass spectrometry method for the online analysis of organic aerosols, Anal. Chem., 76, 2820-2826, 2004.

Hirokawa, J., Kato, T., and Mafune, F.: In situ measurements of atmospheric nitrous acid by chemical ionization mass spectrometry using chloride ion transfer reactions, Anal. Chem., 81, 8380-8386, 2009.

Huey, L. G., Hanson, D. R., and Howard, C. J.: Reactions of SF_6^- and I^- with Atmospheric Trace Gases, J. Phys. Chem., 99, 5001-5008, 1995.

Huey, L. G.: Measurement of trace atmospheric species by chemical ionization mass spectrometry: Speciation of reactive nitrogen and future directions, Mass Spectrom. Rev., 26, 166-184, doi:10.1002/mas.20118, 2007.

Hyttinen, N., Kupiainen-Maatta, O., Rissanen, M. P., Muuronen, M., Ehn, M., and Kurten, T.: Modeling the charging of highly oxidized cyclohexene ozonolysis products using nitrate-based chemical ionization, J. Phys. Chem. A, 119, 6339-6345, doi:10.1021/acs.jpca.5b01818, 2015.

Inomata, S., and Hirokawa, J.: Non-radioactive chemical ionization mass spectrometry using acetic acid-acetate cluster as a reagent ion for the real-time measurement of acids and hydroperoxides, Chem. Lett., 46, 38-41, 2017.

Iyer, S., Lopez-Hilfiker, F., Lee, B. H., Thornton, J. A., and Kurten, T.: Modeling the detection of organic and inorganic compounds using iodide-based chemical ionization, J. Phys. Chem. A, 120, 576-587, doi:10.1021/acs.jpca.5b09837, 2016.

Jokinen, T., Berndt, T., Makkonen, R., Kerminen, V. M., Junninen, H., Paasonen, P., Stratmann, F., Herrmann, H., Guenther, A. B., Worsnop, D. R., Kulmala, M., Ehn, M., and Sipila, M.: Production of extremely low volatile organic compounds from biogenic emissions: Measured yields and atmospheric implications, Proc. Natl. Acad. Sci. U. S. A., 112, 7123-7128, 2015.

Junninen, H., Ehn, M., Petaja, T., Luosujarvi, L., Kotiaho, T., Kostiainen, R., Rohner, U., Gonin, M., Fuhrer, K., Kulmala, M., and Worsnop, D. R.: A high-resolution mass spectrometer to measure atmospheric ion composition, Atmos. Meas. Tech., 3, 1039-1053, 2010.

Kercher, J. P., Riedel, T. P., and Thornton, J. A.: Chlorine activation by N_2O_5: simultaneous, in situ detection of $ClNO_2$ and N_2O_5 by chemical ionization mass spectrometry, Atmos. Meas. Tech., 2, 193-204, 2009.

Kim, M. J., Zoerb, M. C., Campbell, N. R., Zimmermann, K. J., Blomquist, B. W., Huebert, B. J., and Bertram, T. H.: Revisiting benzene cluster cations for the chemical ionization of dimethyl sulfide and select volatile organic compounds, Atmos. Meas. Tech., 9, 1473-1484, 2016.

Kristensen, K., Watne, A. K., Hammes, J., Lutz, A., Petaja, T., Hallquist, M., Bilde, M., and Glasius, M.: High-Molecular weight dimer esters are major products in aerosols from α-pinene ozonolysis and the boreal forest, Environ. Sci. Technol. Lett., 3, 280-285, doi:10.1021/acs.estlett.6b00152, 2016.

575 Laskin, A., Laskin, J., and Nizkorodov, S. A.: Mass spectrometric approaches for chemical
576 characterisation of atmospheric aerosols: critical review of the most recent advances,
577 Environ. Chem., 9, 163-189, doi:10.1071/EN12052, 2012.
578 Lee, B. H., Lopez-Hilfiker, F. D., Mohr, C., Kurten, T., Worsnop, D. R., and Thornton, J. A.: An
579 Iodide-adduct high-resolution time-of-flight chemical-ionization mass spectrometer:
580 Application to atmospheric inorganic and organic compounds, Environ. Sci. Technol., 48,
581 6309-6317, doi:10.1021/es500362a, 2014.
582 Lee, B. H., Mohr, C., Lopez-Hilfiker, F. D., Lutz, A., Hallquist, M., Lee, L., Romer, P., Cohen,
583 R. C., Iyer, S., Kurten, T., Hu, W. W., Day, D. A., Campuzano-Jost, P., Jimenez, J. L.,
584 Xu, L., Ng, N. L., Guo, H. Y., Weber, R. J., Wild, R. J., Brown, S. S., Koss, A., de Gouw,
585 J., Olson, K., Goldstein, A. H., Seco, R., Kim, S., McAvey, K., Shepson, P. B., Starn, T.,
586 Baumann, K., Edgerton, E. S., Liu, J. M., Shilling, J. E., Miller, D. O., Brune, W.,
587 Schobesberger, S., D'Ambro, E. L., and Thornton, J. A.: Highly functionalized organic
588 nitrates in the southeast United States: Contribution to secondary organic aerosol and
589 reactive nitrogen budgets, Proc. Natl. Acad. Sci. U. S. A., 113, 1516-1521,
590 doi:10.1073/pnas.1508108113, 2016.
591 Lopez-Hilfiker, F. D., Mohr, C., Ehn, M., Rubach, F., Kleist, E., Wildt, J., Mentel, T. F., Lutz, A.,
592 Hallquist, M., Worsnop, D., and Thornton, J. A.: A novel method for online analysis of
593 gas and particle composition: description and evaluation of a Filter Inlet for Gases and
594 AEROsols (FIGAERO), Atmos. Meas. Tech., 7, 983-1001, doi:10.5194/amt-7-983-2014,
595 2014.
596 Lopez-Hilfiker, F. D., Mohr, C., Ehn, M., Rubach, F., Kleist, E., Wildt, J., Mentel, T. F.,
597 Carrasquillo, A. J., Daumit, K. E., Hunter, J. F., Kroll, J. H., Worsnop, D. R., and
598 Thornton, J. A.: Phase partitioning and volatility of secondary organic aerosol
599 components formed from alpha-pinene ozonolysis and OH oxidation: the importance of
600 accretion products and other low volatility compounds, Atmos. Chem. Phys., 15, 7765-
601 7776, doi:10.5194/acp-15-7765-2015, 2015.
602 Lopez-Hilfiker, F. D., Iyer, S., Mohr, C., Lee, B. H., D'Ambro, E. L., Kurten, T., and Thornton, J.
603 A.: Constraining the sensitivity of iodide adduct chemical ionization mass spectrometry
604 to multifunctional organic molecules using the collision limit and thermodynamic
605 stability of iodide ion adducts, Atmos. Meas. Tech., 9, 1505-1512, 2016a.
606 Lopez-Hilfiker, F. D., Mohr, C., D'Ambro, E. L., Lutz, A., Riedel, T. P., Gaston, C. J., Iyer, S.,
607 Zhang, Z., Gold, A., Surratt, J. D., Lee, B. H., Kurten, T., Hu, W. W., Jimenez, J.,
608 Hallquist, M., and Thornton, J. A.: Molecular Composition and Volatility of Organic
609 Aerosol in the Southeastern US: Implications for IEPOX Derived SOA, Environ. Sci.
610 Technol., 50, 2200-2209, doi:10.1021/acs.est.5b04769, 2016b.
611 Mohr, C., Lopez-Hilfiker, F. D., Yli-Juuti, T., Heitto, A., Lutz, A., Hallquist, M., D'Ambro, E. L.,
612 Rissanen, M. P., Hao, L. Q., Schobesberger, S., Kulmala, M., Mauldin III, R. L., Ulla
613 Makkonen, U., Sipilä, M., Petäjä, T., Thornton, J. A.: Ambient observations of dimers
614 from terpene oxidation in the gas-phase: implications for new particle formation and
615 growth, Geophys. Res. Lett., doi: 10.1002/2017GL072718, 2017.
616 Nguyen, T. B., Bateman, A. P., Bones, D. L., Nizkorodov, S. A., Laskin, J., and Laskin, A.:
617 High-resolution mass spectrometry analysis of secondary organic aerosol generated by
618 ozonolysis of isoprene, Atmos. Environ., 44, 1032-1042, 2010.

619 Nizkorodov, S. A., Laskin, J., and Laskin, A.: Molecular chemistry of organic aerosols through
620 the application of high resolution mass spectrometry, Phys. Chem. Chem. Phys., 13,
621 3612-3629, doi:10.1039/c0cp02032j, 2011.
622 Noziere, B., Kaberer, M., Claeys, M., Allan, J., D'Anna, B., Decesari, S., Finessi, E., Glasius, M.,
623 Grgic, I., Hamilton, J. F., Hoffmann, T., Iinuma, Y., Jaoui, M., Kahno, A., Kampf, C. J.,
624 Kourtchev, I., Maenhaut, W., Marsden, N., Saarikoski, S., Schnelle-Kreis, J., Surratt, J.
625 D., Szidat, S., Szmigielski, R., and Wisthaler, A.: The Molecular Identification of
626 Organic Compounds in the Atmosphere: State of the Art and Challenges, Chem. Rev.,
627 115, 3919-3983, doi:10.1021/cr5003485, 2015.
628 Praplan, A. P., Schobesberger, S., Bianchi, F., Rissanen, M. P., Ehn, M., Jokinen, T., Junninen,
629 H., Adamov, A., Amorim, A., Dommen, J., Duplissy, J., Hakala, J., Hansel, A., Heinritzi,
630 M., Kangasluoma, J., Kirkby, J., Krapf, M., Kurten, A., Lehtipalo, K., Riccobono, F.,
631 Rondo, L., Sarnela, N., Simon, M., Tome, A., Trostl, J., Winkler, P. M., Williamson, C.,
632 Ye, P., Curtius, J., Baltensperger, U., Donahue, N. M., Kulmala, M., and Worsnop, D. R.:
633 Elemental composition and clustering behaviour of alpha-pinene oxidation products for
634 different oxidation conditions, Atmos. Chem. Phys., 15, 4145-4159, 2015.
635 Seinfeld, J. H., and Pandis, S. N.: Atmospheric chemistry and physics: from air pollution to
636 climate change, 2nd ed., J. Wiley, Hoboken, N.J., 2006.
637 Smith, J. N., Moore, K. F., McMurry, P. H., and Eisele, F. L.: Atmospheric measurements of
638 sub-20 nm diameter particle chemical composition by thermal desorption chemical
639 ionization mass spectrometry, Aerosol Sci. Technol., 38, 100-110,
640 doi:10.1080/02786820490249036, 2004.
641 Trostl, J., Chuang, W. K., Gordon, H., Heinritzi, M., Yan, C., Molteni, U., Ahlm, L., Frege, C.,
642 Bianchi, F., Wagner, R., Simon, M., Lehtipalo, K., Williamson, C., Craven, J. S.,
643 Duplissy, J., Adamov, A., Almeida, J., Bernhammer, A. K., Breitenlechner, M., Brilke, S.,
644 Dias, A., Ehrhart, S., Flagan, R. C., Franchin, A., Fuchs, C., Guida, R., Gysel, M., Hansel,
645 A., Hoyle, C. R., Jokinen, T., Junninen, H., Kangasluoma, J., Keskinen, H., Kim, J.,
646 Krapf, M., Kurten, A., Laaksonen, A., Lawler, M., Leiminger, M., Mathot, S., Mohler, O.,
647 Nieminen, T., Onnela, A., Petaja, T., Piel, F. M., Miettinen, P., Rissanen, M. P., Rondo,
648 L., Sarnela, N., Schobesberger, S., Sengupta, K., Sipila, M., Smith, J. N., Steiner, G.,
649 Tome, A., Virtanen, A., Wagner, A. C., Weingartner, E., Wimmer, D., Winkler, P. M.,
650 Ye, P. L., Carslaw, K. S., Curtius, J., Dommen, J., Kirkby, J., Kulmala, M., Riipinen, I.,
651 Worsnop, D. R., Donahue, N. M., and Baltensperger, U.: The role of low-volatility
652 organic compounds in initial particle growth in the atmosphere, Nature, 533, 527-531,
653 doi:10.1038/nature18271, 2016.
654 Tu, P. J., Hall, W. A., and Johnston, M. V.: Characterization of Highly Oxidized Molecules in
655 Fresh and Aged Biogenic Secondary Organic Aerosol, Anal. Chem., 88, 4495-4501, 2016.
656 Veres, P., Roberts, J. M., Warneke, C., Welsh-Bon, D., Zahniser, M., Herndon, S., Fall, R., and
657 de Gouw, J.: Development of negative-ion proton-transfer chemical-ionization mass
658 spectrometry (NI-PT-CIMS) for the measurement of gas-phase organic acids in the
659 atmosphere, Int. J. Mass Spectrom., 274, 48-55, 2008.
660 Witkowski, B., and Gierczak, T.: Analysis of alpha-acyloxyhydroperoxy aldehydes with
661 electrospray ionization-tandem mass spectrometry (ESI-MS^n), J. Mass Spectrom., 48, 79-
662 88, doi:10.1002/jms.3130, 2013.
663 Yatavelli, R. L. N., Lopez-Hilfiker, F., Wargo, J. D., Kimmel, J. R., Cubison, M. J., Bertram, T.
664 H., Jimenez, J. L., Gonin, M., Worsnop, D. R., and Thornton, J. A.: A Chemical

Ionization High-Resolution Time-of-Flight Mass Spectrometer Coupled to a Micro Orifice Volatilization Impactor (MOVI-HRToF-CIMS) for Analysis of Gas and Particle-Phase Organic Species, Aerosol Sci. Technol., 46, 1313-1327, doi:10.1080/02786826.2012.712236, 2012.

Yuan, B., Koss, A., Warneke, C., Gilman, J. B., Lerner, B. M., Stark, H., and de Gouw, J. A.: A high-resolution time-of-flight chemical ionization mass spectrometer utilizing hydronium ions (H_3O^+ ToF-CIMS) for measurements of volatile organic compounds in the atmosphere, Atmos. Meas. Tech., 9, 2735-2752, doi:10.5194/amt-9-2735-2016, 2016.

Zhao, J., Eisele, F. L., Titcombe, M., Kuang, C. G., and McMurry, P. H.: Chemical ionization mass spectrometric measurements of atmospheric neutral clusters using the cluster-CIMS, J. Geophys. Res., 115, 2010.

Zhao, J., Ortega, J., Chen, M., McMurry, P. H., and Smith, J. N.: Dependence of particle nucleation and growth on high-molecular-weight gas-phase products during ozonolysis of alpha-pinene, Atmos. Chem. Phys., 13, 7631-7644, 2013.

Zhao, Y., Wingen, L. M., Perraud, V., Greaves, J., and Finlayson-Pitts, B. J.: Role of the reaction of stabilized Criegee intermediates with peroxy radicals in particle formation and growth in air, Phys. Chem. Chem. Phys., 17, 12500-12514, doi:10.1039/C5cp01171j, 2015.

Zhao, Y., Wingen, L. M., Perraud, V., and Finlayson-Pitts, B. J.: Phase, composition, and growth mechanism for secondary organic aerosol from the ozonolysis of α-cedrene, Atmos. Chem. Phys., 16, 3245-3264, 2016.

Atmos. Meas. Tech. Discuss., doi:10.5194/amt-2017-83, 2017
Manuscript under review for journal Atmos. Meas. Tech.
Discussion started: 30 March 2017

Atmospheric Measurement Techniques Discussions

687

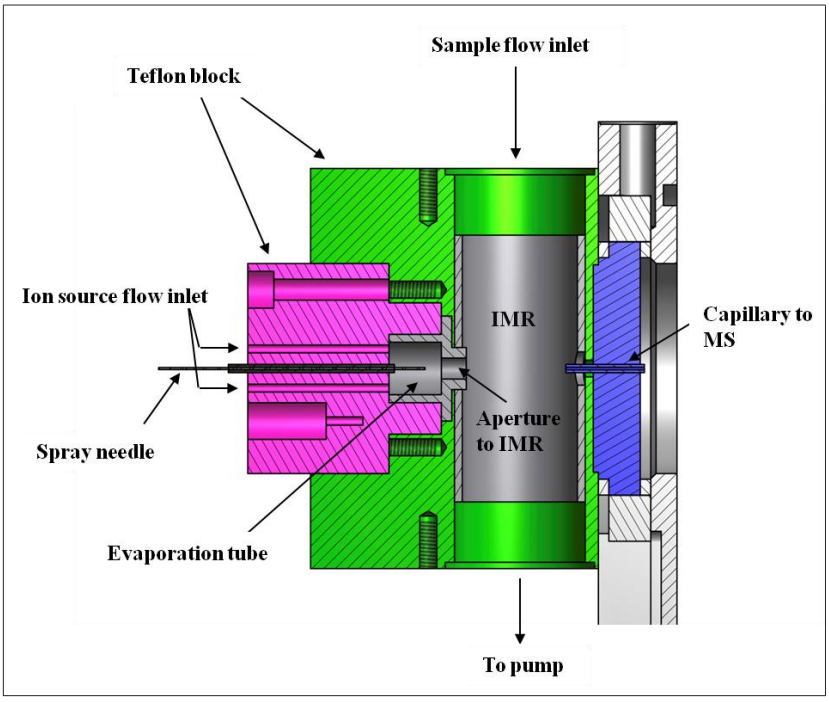

688

689 **Figure 1** Schematic of the electrospray chemical ionization (ESCI) source module. Also shown
690 are the orthogonal atmospheric pressure IMR and the entrance capillary serving as the
691 atmospheric pressure interface between the IMR and the vacuum chamber of HRToF-MS. See
692 text for detailed description of the source.

693

694

695

696

697

Atmos. Meas. Tech. Discuss., doi:10.5194/amt-2017-83, 2017
Manuscript under review for journal Atmos. Meas. Tech.
Discussion started: 30 March 2017

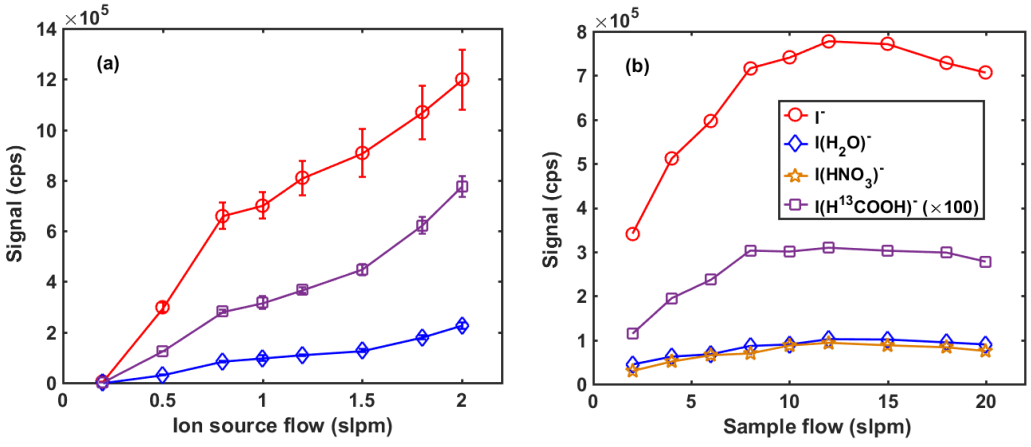

Figure 2 Dependence of ion signals on the ion source flow and sample flow. (a) Ion signals observed as a function of ion source flow during the sampling of humid room air (15 mbar water vapor pressure) containing $H^{13}COOH$ at a flow of 10 slpm. (b) Ion signals observed during the sampling of humid room air containing $H^{13}COOH$ and HNO_3 gat flow rates of 2-20 slpm (the ratio of ion source flow/sample flow is fixed to be 1:10). The signals for $I(H^{13}COOH)^-$ in (a) and (b) are magnified by 100 times.

Atmos. Meas. Tech. Discuss., doi:10.5194/amt-2017-83, 2017
Manuscript under review for journal Atmos. Meas. Tech.
Discussion started: 30 March 2017

Atmospheric Measurement Techniques Discussions

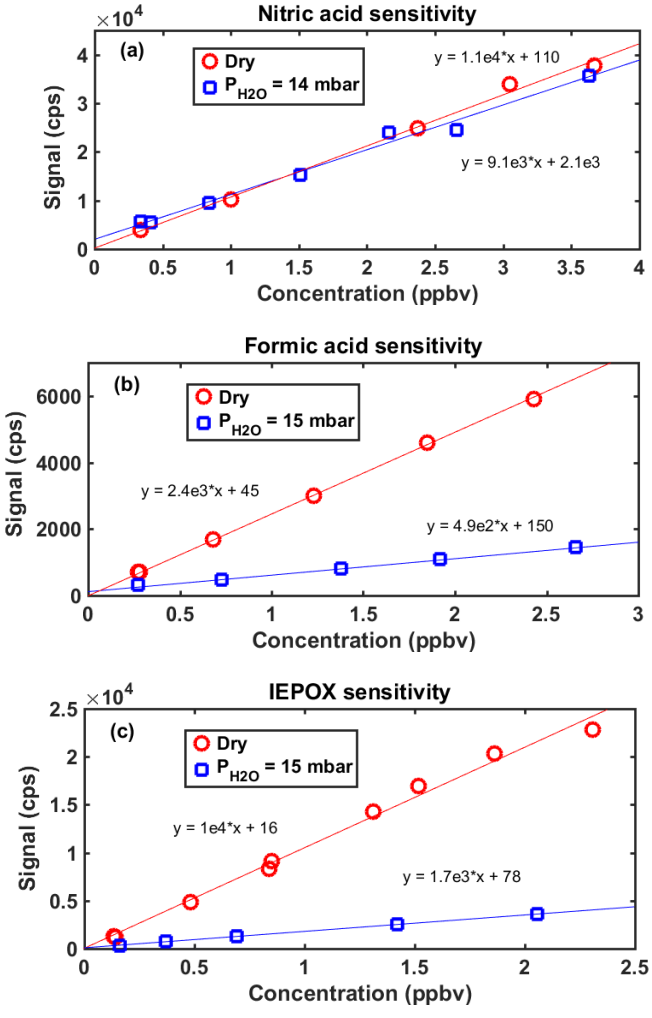

Figure 3 Normalized sensitivity to (a) nitric acid, (b) formic acid, and (c) IEPOX under dry and humid (14 or 15 mbar water vapor pressure) conditions. Signals are normalized by the ratio of observed total reagent ion count rates to a million ion count rate. The normalized signals were observed to be a linear function of the delivered concentration. The slope derived from a linear fit corresponds to the sensitivity per million reagent ion count rates.

Atmos. Meas. Tech. Discuss., doi:10.5194/amt-2017-83, 2017
Manuscript under review for journal Atmos. Meas. Tech.
Discussion started: 30 March 2017

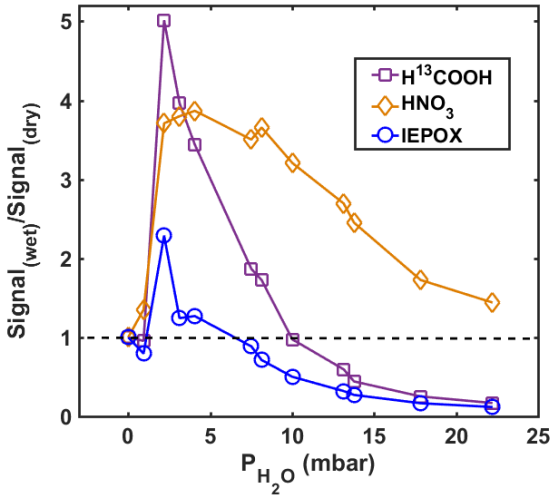

715

716 **Figure 4** Normalized signal of $I(HNO_3)^-$, $I(H^{13}COOH)^-$, and $I(IEPOX)^-$ as a function of water
717 vapor pressure (P_{H2O}) in the IMR. The signal of iodide-analyte clusters is first normalized by the
718 total regent ion (I^- and $I(H_2O)^-$) signals. The resulting normalized signal at each P_{H2O} was then
719 normalized again to the respective value under dry conditions (P_{H2O} = 0, dry UHP N_2).

720

Atmos. Meas. Tech. Discuss., doi:10.5194/amt-2017-83, 2017
Manuscript under review for journal Atmos. Meas. Tech.
Discussion started: 30 March 2017

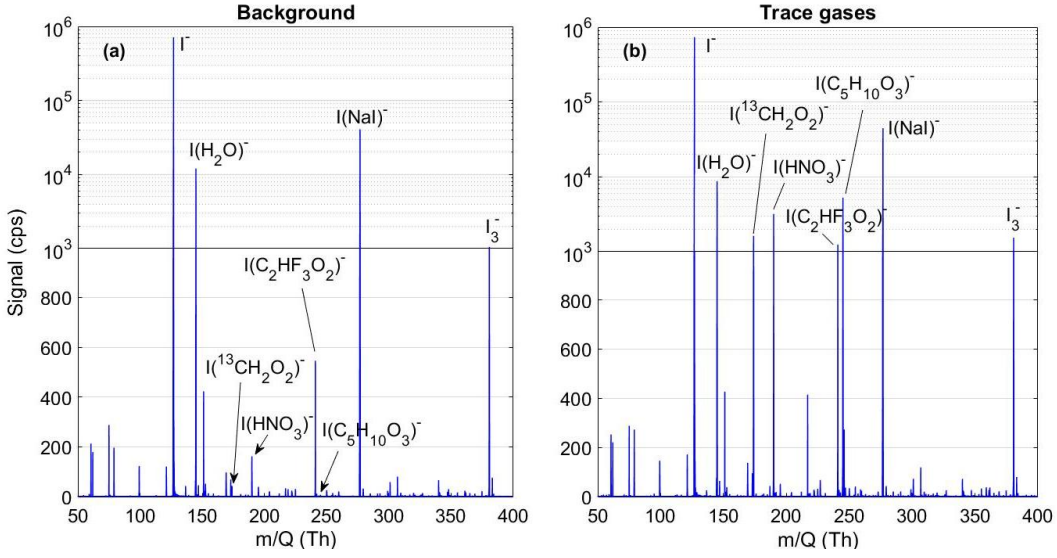

721

722 **Figure 5** High resolution mass spectra collected when sampling (a) UHP N_2 and (b) UHP N_2
723 containing HNO_3, $H^{13}COOH$, and IEPOX gases.

724

Atmos. Meas. Tech. Discuss., doi:10.5194/amt-2017-83, 2017
Manuscript under review for journal Atmos. Meas. Tech.
Discussion started: 30 March 2017

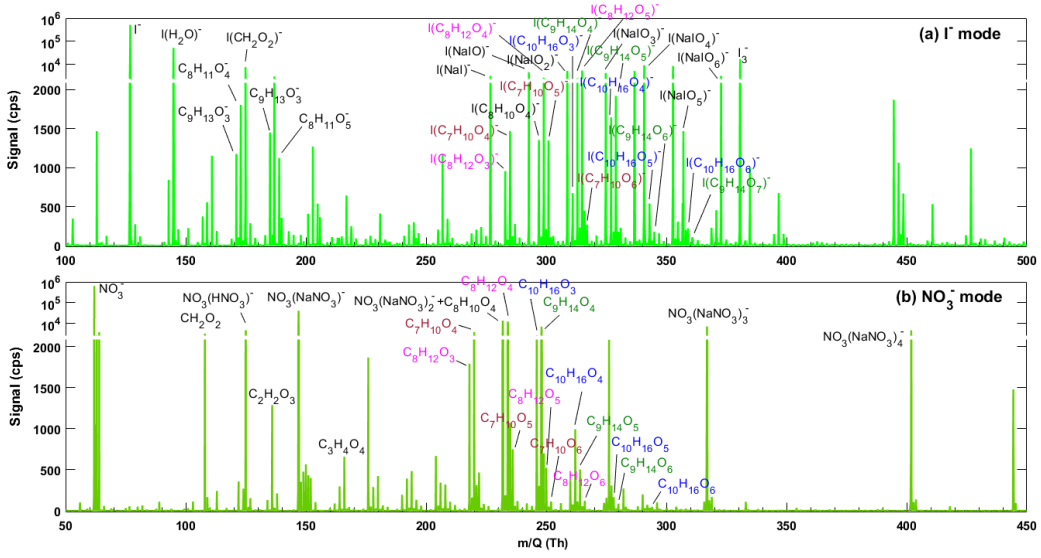

Figure 6 High resolution mass spectra obtained during ozonolysis of α-pinene in a steady-state chamber using (a) I^- and (b) NO_3^- modes. For NO_3^- mode, the chemical formulae of organic ion clusters are shown without the corresponding NO_3^- adduct for clarity as, unlike I^- mode, organic ions without a NO_3^- adduct were negligible components of the spectrum.

Atmos. Meas. Tech. Discuss., doi:10.5194/amt-2017-83, 2017
Manuscript under review for journal Atmos. Meas. Tech.
Discussion started: 30 March 2017

Atmospheric Measurement Techniques Discussions

731

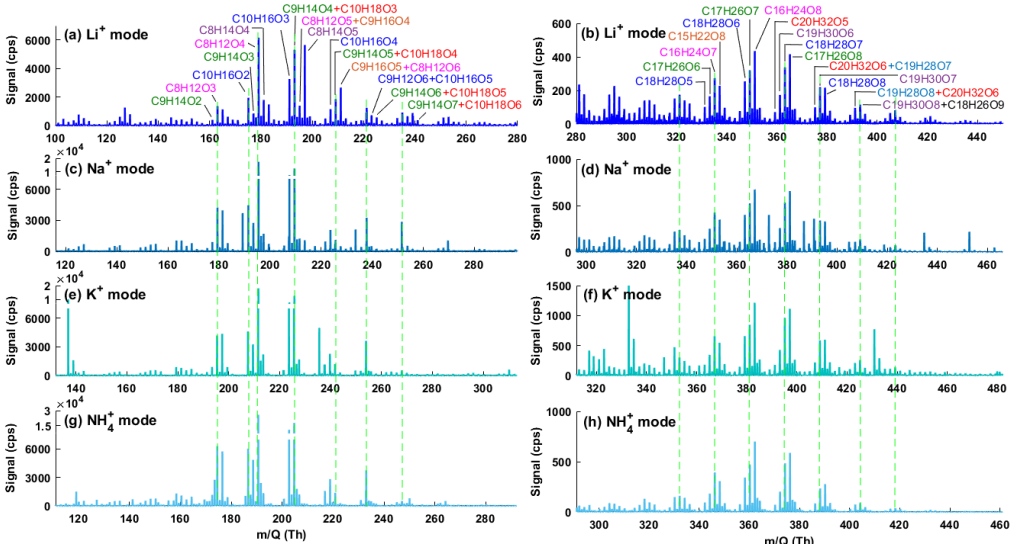

732

733 **Figure 7** High resolution mass spectra of α-pinene ozonolysis products in (a, c, e, g) monomers
734 and (b, d, f, h) dimers regions observed in (a, b) Li^+ mode, (c, d) Na^+ mode, (e, f) K^+ mode, and
735 (g, h) NH_4^+ mode. The chemical formulae of the detected organics are given for major peaks
736 observed in the mass spectra. To allow direct comparison, the reagent ion adduct has been
737 removed from the detected cluster in each spectrum.

738

Atmos. Meas. Tech. Discuss., doi:10.5194/amt-2017-83, 2017
Manuscript under review for journal Atmos. Meas. Tech.
Discussion started: 30 March 2017

Atmospheric Measurement Techniques Discussions

739

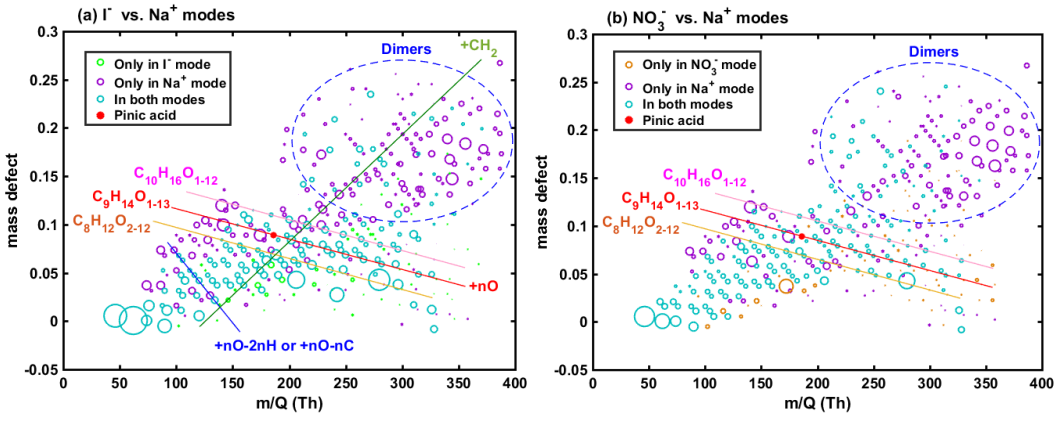

740

741 **Figure 8** Comparisons of mass defect plots derived in (a) I^- and Na^+ modes, and (b) NO_3^- and
742 Na^+ modes during ozonolysis of α-pinene in a steady-state chamber. To compare the mass defect
743 plot obtained in two different ion modes, the reagent ions in observed clusters are excluded for
744 the mass defect calculation, and the signals are normalized to the corresponding pinic acid
745 intensity in each mode (see text for details). The purple circles do not necessarily mean such ions
746 were undetected in the negative mode as they may have very small signal (< 5 cps) and be
747 excluded for the high-resolution fitting.

748

Atmos. Meas. Tech. Discuss., doi:10.5194/amt-2017-83, 2017
Manuscript under review for journal Atmos. Meas. Tech.
Discussion started: 30 March 2017

Atmospheric Measurement Techniques Discussions

749

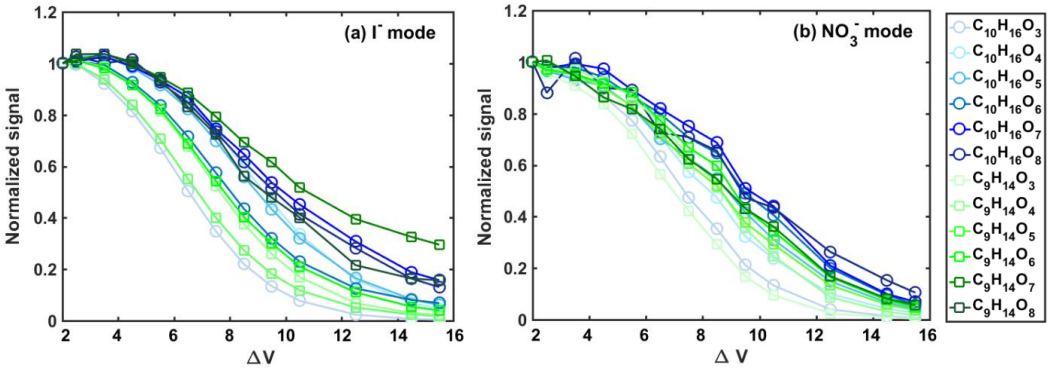

750

751 **Figure 9** Declustering scans of products $C_{10}H_{16}O_{2\text{-}8}$ and $C_9H_{14}O_{3\text{-}8}$ formed by the ozonolysis of
752 α-pinene in (a) I^- and (b) NO_3^- modes. ΔV denotes the voltage differences between the end of
753 first and the entrance to the second quadrupole sections of the mass spectrometer. Signals at
754 each ΔV are normalized to that obtained at the weakest declustering strength (i.e., ΔV= 2 V).

755

Atmos. Meas. Tech. Discuss., doi:10.5194/amt-2017-83, 2017
Manuscript under review for journal Atmos. Meas. Tech.
Discussion started: 30 March 2017

Atmospheric Measurement Techniques Discussions

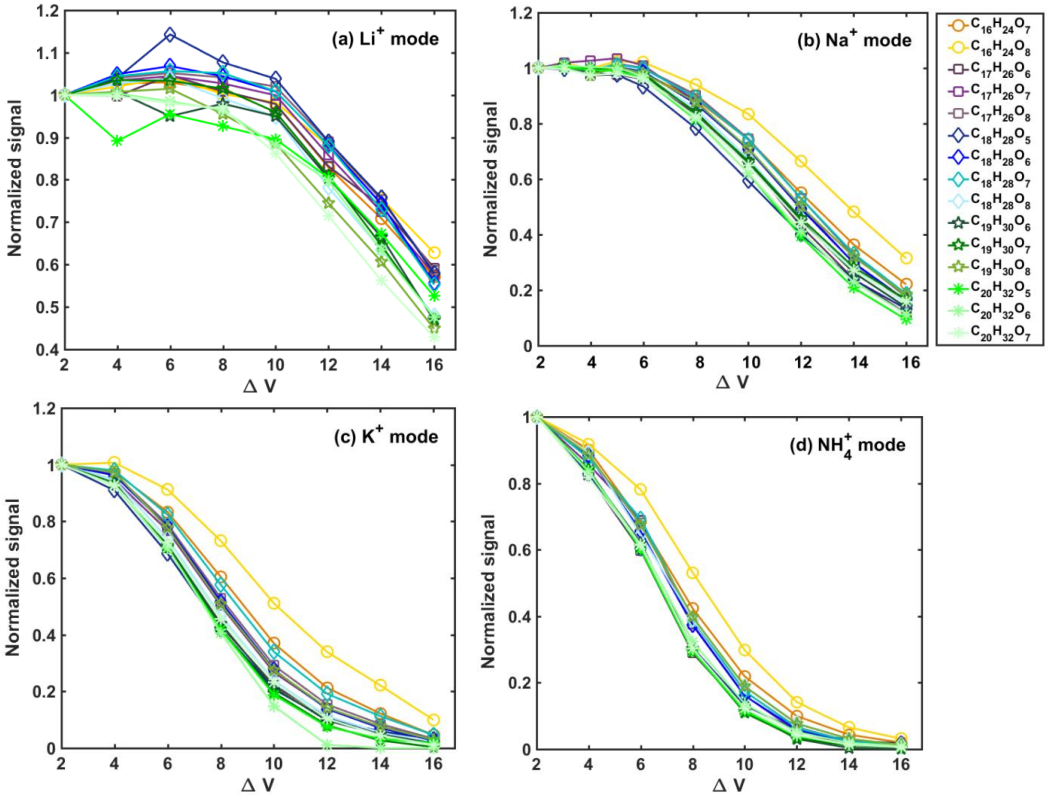

Figure 10 Declustering scans of 15 most abundant dimers formed by the ozonolysis of α-pinene in (a) Li^+ mode, (b) Na^+ mode, (c) K^+ mode, and (d) NH_4^+ mode. ΔV denotes the voltage differences between the first and second quadrupole sections of the mass spectrometer. Signals at each ΔV are normalized to that obtained at the weakest declustering strength (i.e., ΔV= 2 V).